SYNTHESIZING THERMAL BACKGROUNDS FROM VISIBLE-SWIR SPECTRAL IMAGERY FOR USE IN EARTH SCENE SIMULATIONS

Robert Sundberg and Timothy Perkins

Spectral Sciences Inc, 30 Fourth Avenue, Suite 2, Burlington, MA 01803, USA

ABSTRACT

This paper examines the utility of synthetic spectral imagery derived from visible-SWIR HSI or MSI sensor data. Our method uses an endmember matching approach to extend spectral information to wavelengths beyond the original imagery. The derived images exhibit some loss of spectral and spatial clutter, but the dimensionality may be sufficient for applications such as synthetic scene simulations and development of algorithms for object detection.

Index Terms— Scene Simulation, Thermal Imagery, Hyperspectral, Multispectral, Remote Sensing

1. INTRODUCTION

This paper discusses the development of a technique for generating Earth terrains for use in a robust 3D spectral imaging scene simulator. A major challenge in scene simulation is to build in sufficient complexity, or "clutter", in both the spatial and spectral domains of the reflectance or emissivity/temperature image data. This detail is extremely important for evaluating object detection algorithms. An oversimplified scene will present an unrealistically benign background for matched filter, subspace projection, and other algorithms, resulting in overly optimistic estimates for detection performance. Therefore, a practical difficulty when creating a complex scene is the large quantity of user input required to represent natural variations of objects and materials throughout the scene, which includes distributions of spectral reflectance, emissivity, and temperature for each object. We have developed a procedure for synthesizing a realistic hyperspectral or multi-spectral reflectance cube at arbitrary wavelengths covering visible through LWIR wavelengths using a VIS/SWIR spectral image as a template. The result can serve as the starting point for a radiance image simulation model, such as MCScene [1,2].

The concept underlying the procedure is to find a representation of spectral VIS/SWIR image data in terms of a library of reflectance spectra that extends from the visible to the LWIR. Temperatures are then assigned based on material type and degree of solar shading. The resulting reflectance cube and temperature map can be used to simulate radiance cubes for any set of sensor and atmosphere parameters. Accurate and realistically simulated hyperspectral imagery can provide a practical alternative to field measurements for the evaluation of algorithms under a wide variety of atmospheric and surface conditions.

Recent advances have been made using machine learning approaches from conversion of visible imagery into thermal images. Several approaches for visible to thermal image conversion [3-6] have employed a generative adversarial network (GAN) [7] approach where the model is trained using matched visible and thermal image pairs. These models have been developed for RGB visible imagery converted to broad band thermal images. Such approaches may work for converting multi- or hyperspectral visible imagery to multi- or hyperspectral thermal imagery but would require many matched pair spectral images for training. It is uncommon to have matched hyperspectral image pairs in measured data although there may be approaches for synthetic generation of such scenes [3]. There are multispectral imagery collects by the MODIS/ASTER Airborne Simulator (MASTER) [8] airborne scanning spectrometer which provides 25 visible-SWIR spectral bands and 25 spatially matched MWIR-LWIR spectral bands. This airborne platform collects data with ground sampling distances (GSD) from 5 to 50 m in size which may be too large for some object detection applications [9]. The use of machine learning in the conversion of multi- or hyperspectral imagery to multi- or hyperspectral thermal imagery is currently under investigation [10].

Section 2 describes the technical approach of creating thermal emissivity maps from spectral visible-SWIR imagery. We also briefly discuss methods to measure the spectral and spatial variability in terms of scene statistics. In Section 3 we evaluate some example thermal backgrounds resulting from our method. To further test the approach, we also analyze the spectral complexity of the scene by inserting spectrally similar and dissimilar targets into the synthetic scene and determining receiver-operator characteristic (ROC) curves using ACE [11] spectral detection in the original visible-SWIR scenes as well as the derived visible-SWIR, MWIR and LWIR scenes.

2. SPECTRAL BACKGROUND GENERATION

2.1 Approach

In the first step of the procedure, a visible-SWIR radiance cube is corrected for atmospheric (AC) effects [12-14]. Next

a large spectral library of reflectance materials which covers the full visible to LWIR spectral range [15] is resampled to the same spectral band positions and widths as the input data cube. This spectrally reduced library is used with an unmixing method [16,17] to determine the abundance of each endmember in the library for every pixel in the scene. Using the abundance maps and the full-spectrum spectral library, the scene is reconstituted to form a spectral data cube in the desired spectral domain.

This approach clearly doesn't produce reflectivity or emissivity maps that would be an exact match to the actual scene. For example, a visible-SWIR pixel that is identified as building cement will not necessarily have the correct emissivity for that exact type of material, but the emissivity of a similar type of material, cement in this case. The resulting scenes should however carry an equivalent spectral dimensionality from the variety of materials present in the visible-SWIR scene and spatial clutter statistics similar to the original vis-SWIR data. This paper later evaluates the ability of the approach to produce realistic estimates of MWIR and LWIR emissivity.

2.2 Measures of Scene Statistics

2.2.1 Spatial Autocorrelation

Spatial autocorrelation is used to describe the extent to which a pixel is correlated across a scene with the nearby pixels. Positive spatial autocorrelation occurs when pixels with similar values are closer together, clustered. Negative spatial autocorrelation occurs when observations with dissimilar values are closer together. Spatial autocorrelation is often assessed using indices that summarize the degree to which similar observations tend to occur near each other. The Moran's I (MI) [18] index is a common measure where a value near one indicates positive correlation, a value near zero indicates the lack of correlation and a negative value indicates negative correlation between adjacent pixels.

The spatial correlation of spectral scenes will vary for each spectral band. Since we are comparing MI index for various spectral domains we will use an average value across all bands in the data for a given scene. For our purposes it is important for the synthetic data to maintain a similar value for the MI index as the original data.

2.2.2 Spectral Measures

We have examined four criteria found in the literature for determining the dimensionality of a data set. We have avoided a common technique, called the Scree Test [19], because it requires one to plot the variance of the principal components (PC) as a function of component number to identify a clear change in slope. This technique was judged to be too arbitrary.

PC Eigenvalues Above the Noise

There are several methods which attempt to estimate the noise level in a scene and define the dimensionality as those PC eigenvalues above the noise floor. Recent work by Thompson et al. [20], has examined the dimensionality of AVIRIS data from 600 flightlines collected over a variety of terrain types and pixel GSDs in 2013 to 2014. In their technique they develop an estimate of the noise in the down-track direction of the imagery by calculating the difference between the original PC image and a smoothed version of the PC image. The scene dimensionality is the last PC eigenvalue index for which the standard deviation of the signal image exceeds the standard deviation of the noise image. In their work using the AVIRIS data they used a 1-D local average over 11 pixels. The choice of 11-pixel smoothing was based on the spatial uniformity of the AVIRIS instrument. The size of the smoothing window is sensor specific making this measure more difficult for comparing values from one sensor to another.

Cumulative Variability (CV)

In this approach the image is transformed to principal components and the cumulative variance of the principal component expansion is determined. A threshold is selected, typically 90% or 95% of the variance is used, and the number of principal components required to reach this threshold defines the dimensionality.

Continuous Significant Dimensionality (CSD)

This criterion uses the eigenvalues of the correlation matrix in the following sum:

$$\mathrm{CSD} = \sum_{j=1}^{m} \min(\lambda_j,\ 1.0)$$

where λ_j is the jth eigenvalue of the correlation matrix and m is the total number of vectors. The correlation matrix is equivalent to the covariance matrix for an image where each band has been standardized to zero mean and unit variance. The CSD is equal to the linear dimensionality of a set of variables and is equal to the number of variables in an orthogonal basis [21].

Variances of the Correlation Principal Components

This criterion is based on the selection of PC using the correlation matrix. One selects a threshold and counts the number of PC eigenvalues greater than the threshold. Typically, a threshold of 1.0 [22] or 0.7 [23] is selected.

2.2.3 Testing Spectral Dimensionality Measures

To evaluate these criteria for the dimensionality of a scene we have created a simple test problem. We have defined 100 orthogonal vectors and have created a 256 by 256 image using these vectors in random linear combinations. The vectors have 200 "spectral" channels. The results for the above criteria and Singular Value Decomposition (SVD) are summarized in Table 1. The method suggested by Thompson was not included here because of the random nature of the spectral signatures would make a noise estimate meaningless. We have also examined the addition of Gaussian random noise to our model problem. Table 1 includes noise at levels of 0, 5, 10 and 20%.

For this simple test case we can see some of the usefulness, or lack thereof, of some of the measures. SVD for example, provides a mathematical definition of the dimensionality that would not prove very useful in our simulations work. Perhaps the most useful measure is the CSD measure, which increased monotonically as the noise level increased forming a reasonable measure of the spectral complexity. CSD will be used in comparing our derived scenes and the original scene spectral dimensionality.

Table 1. Measures of Dimensionality for Simple Model.

Noise Level	CV (90%)	CSD	Variance of the Correlation PCs Threshold=1.0	Threshold = 0.6	SVD
0%	87	99	99	99	100
5%	90	103	99	99	200
10%	95	112	99	99	200
20%	117	131	99	113	200

3. EXAMPLE SCENES

In this section, we use three different visible-SWIR scenes which have different spatial and spectral characteristics to develop higher spectral resolutions visible-SWIR imagery, as well as MWIR and LWIR imagery. Spatial and spectral measures are summarized in Table 2 and discussed in the next section.

3.1 AVIRIS Jasper Ridge

The AVIRIS data collected over Jasper Ridge, CA in 1997 has 224 bands from 0.37 to 2.5 µm. In Figure 1 we illustrate the spectral content of the generated MWIR and LWIR emissivities for vegetation, a road and a dirt pixel.

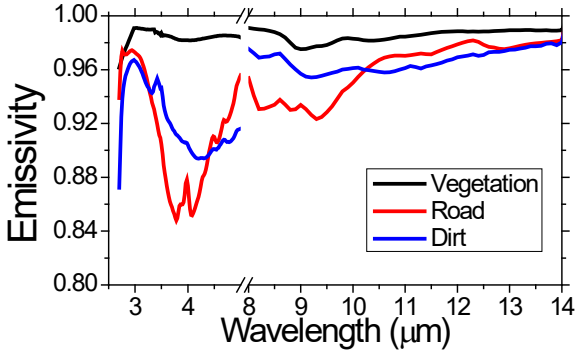


Figure 1. Representative derived emissivities in MWIR and LWIR.

3.2 Sentinel-2 Imagery Near Brisbane

The Sentinel-2 data is from an image west of Brisbane Australia. We have used the four RGB and NIR bands which have a GSD of 10 m along with the two SWIR bands which have a GSD of 20 m. The Sentinel-2 data has been atmospherically compensated using QUAC [12] and resampled to 10 m GSD for all bands. In Figure 2 we show the RGB visible image along with generated MWIR and LWIR emissivity maps. In Figure 3 we illustrate the spectral content of the atmospherically compensated Sentinel-2 (symbols) scene and generated visible-SWIR reflectance, MWIR and LWIR emissivities for vegetation, dirt and a lake pixel.

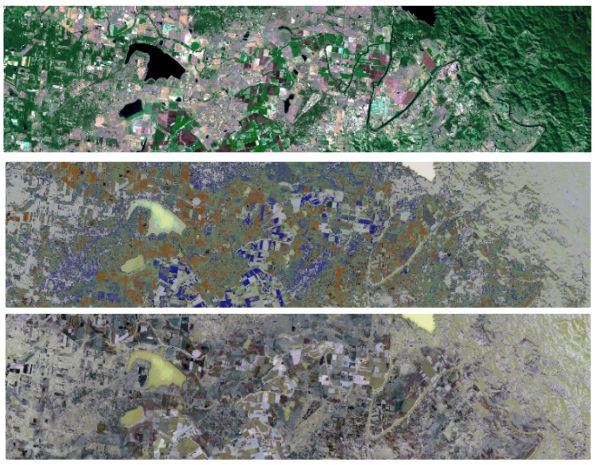


Figure 2. RGB (top), MWIR (3.5,4.,4.5µm) and LWIR (8,10,12 µm) images of Sentinel-2 imagery near Brisbane.

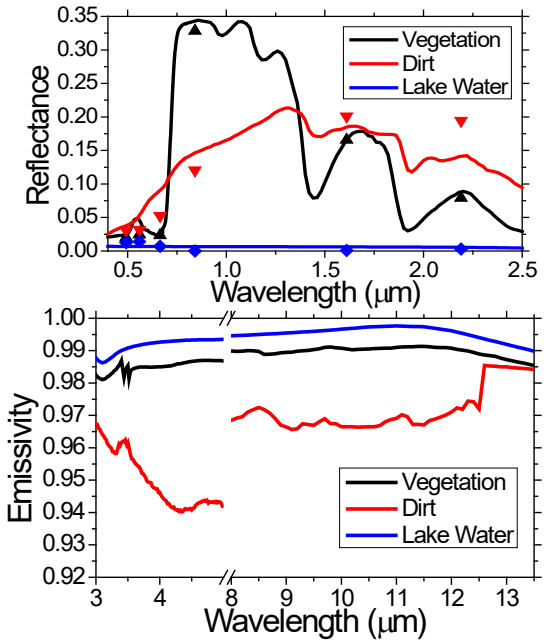


Figure 3. Representative derived reflectance (top) in VSWIR and emissivities (bottom) in MWIR and LWIR.

3.3 WorldView-3 Imagery in Italy

In Figure 4 we show the spectral content of the AC multispectral WV3 (symbols) scene and generated visible-SWIR reflectance, MWIR and LWIR emissivities for vegetation, road, car and roof pixel. The RGB and near Infrared (NIR) imagery was provided by European Space Agency's under the Third Party Missions program.

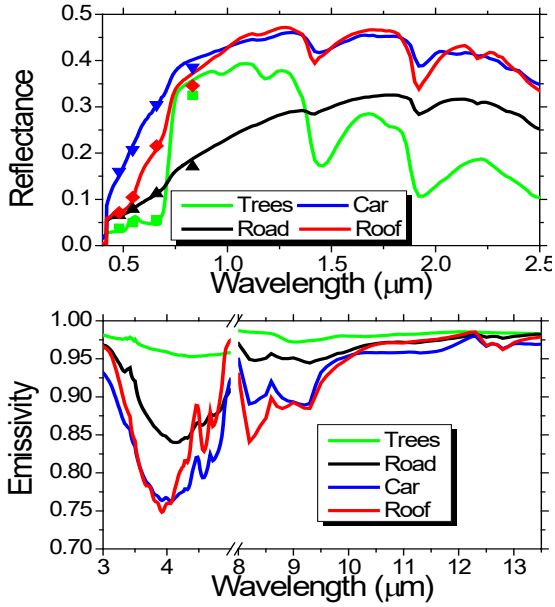


Figure 4. Representative derived reflectance (top) in VSWIR and emissivities (bottom) in MWIR and LWIR.

Table 2. Summary of statistical measures.

Scene	GSD (m)	# Bands	CSD	Moran's I	
				Lag 1	Lag 20
Jasper Ridge	**18**				
Original		224	15.8	0.85	0.42
QUAC VSWIR		209	6.9	0.89	0.44
MWIR		119	4.2	0.71	0.28
LWIR		65	4.5	0.52	0.19
Sentinel-2	**10**				
MSI VSWIR		6	2.9	0.94	0.44
HSI VSWIR		286	7.5	0.92	0.39
MWIR		119	4.8	0.88	0.36
LWIR		65	3.9	0.71	0.21
WorldView-3	**0.6**				
MSI VNIR		4	2.1	0.97	0.45
HSI VSWIR		286	6.6	0.94	0.36
MWIR		119	3.5	0.87	0.32
LWIR		65	2.5	0.83	0.25

3.4 Discussion on Statistics

The CSD and MI statistics show similar trends for the three scenes. The spectral dimensionality is reduced when using HSI data and producing spectral data. When starting with MSI data the spectral dimensionality is increased when producing spectral data. The increase in dimensionality may reflect the capture of noise in the endmember fitting process as well as the fitting residual error.

The MI statistic shows a decrease in spatial correlation as the new spectral scenes are generated, but still a significant correlation between adjacent pixels.

4. ACE TARGET DETECTION RESULTS

To demonstrate the fidelity of the generated spectral reflectivity and emissivity maps we examined the target detection statistics for the three scenes in all the spectral domains. 400 subpixel orange fiberglass signatures were embedded in the three scenes with varying fill-factor from 2% to 10%. The standard Adaptive Coherence Estimator (ACE) [24] detector was used to evaluate detection performance for the generated scenes. Figure 5 shows the ROC curves for the detection of the 400 subpixel targets. The top panel shows the ROC curves for the original AVIRIS data as well as the three derived scenes. Detection is easier with the derived scenes indicating that the derived scenes are spectrally less complicated than the original scene. This result is consistent with the CSD results in Table 2. The middle panel shows the ROC curves for the Sentinel-2 scene and the bottom panel shows the results for the WV3 scene.

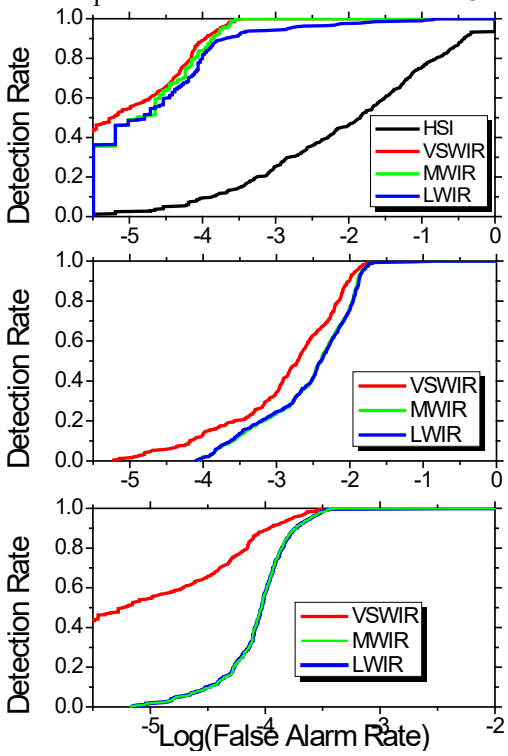


Figure 5. ROC curves showing the detection of the orange fiberglass subpixel target in the derived imagery for the three scenes.

5. SUMMARY

This paper has examined the spectral and spatial scene complexity when spectral scenes are derived from visible-SWIR or VNIR HSI and MSI imagery using an endmember approach to "fill in" spectral information not contained in the original image. The results indicate that derived scenes may be used as scene backgrounds for synthetic imagery but there is some loss of spectral and spatial clutter as compared to the original scenes.

6. REFERENCES

[1] S.C. Richtsmeier, A. Berk, S. Adler-Golden, and L. Bernstein, "A 3D Radiative-Transfer Hyperspectral Image Simulator for Algorithm Validation," *Proceedings of ISSSR 2001*, Quebec City, Canada (June 2001).

[2] R. L. Sundberg, A. Berk, S. C. Richtsmeier, S.M. Adler-Golden, and R. Haren, "Hyperspectral scene simulation from the visible through the LWIR," in the SPIE *proceedings, Sensors, Systems, and Next-Generation Satellites VII*, Vol. 5234, 2003

[3] Uddin, M.S.; Kwan, C.; Li, J. MWIRGAN: Unsupervised Visible-to-MWIR Image Translation with Generative Adversarial Network. *Electronics* 2023, *12*, 1039. https://doi.org/10.3390/electronics12041039

[4] L. Zhang, A. Gonzalez-Garcia, J. van de Weijer, M. Danelljan and F. S. Khan, "Synthetic Data Generation for End-to-End Thermal Infrared Tracking," in *IEEE Transactions on Image Processing*, vol. 28, no. 4, pp. 1837-1850, April 2019, doi: 10.1109/TIP.2018.2879249.

[5] Abbott, R.; Robertson, N.M.; Martinez del Rincon, J.; Connor, B. Unsupervised Object Detection via LWIR/RGB Translation. In *Proceedings of the IEEE/CVF Conference on Computer Vision and Pattern Recognition Workshops*, Seattle, WA, USA, 14–16 June 2020; pp. 90–91.

[6] Kniaz, V.V.; Knyaz, V.A.; Hladuvka, J.; Kropatsch, W.G.; Mizginov, V. Thermalgan: Multimodal color-to-thermal image translation for person re-identification in multispectral dataset. In *Proceedings of the European Conference on Computer Vision (ECCV)*, Munich, Germany, 8–14 September 2018.

[7] Goodfellow, I., Pouget-Abadie, J., Mirza, M., Xu, B., Warde-Farley, D., Ozair, S., Bengio, Y. (2014). *Generative adversarial nets*. In Advances in neural information processing systems (pp. 2672–2680).

[8] Hook, S. J. Myers, J. J., Thome, K. J., Fitzgerald, M. and A. B. Kahle, "The MODIS/ASTER airborne simulator (MASTER) - a new instrument for earth science studies," *Remote Sensing of Environment*, vol. 76, Issue 1, pp. 93-102 (2001).

[9] Zambanini, S.; Loghin, A.-M.; Pfeifer, N.; Soley, E.M.; Sablatnig, R. Detection of Parking Cars in Stereo Satellite Images. *Remote Sens.* **2020**, *12*, 2170. https://doi.org/10.3390/rs12132170

[10] E. Brewer private communication, November 2024.

[11] S.S. Kraut, L.L. Scharf, and R.W. Butler, "The Adaptive Coherence Estimator: A uniformly most-powerful invariant adaptive detection statistic," *IEEE Trans. Signal Processing*, Vol. 53, No. 2 (2005).

[12] L.S. Bernstein, X. Jin, B. Gregor, and S. Adler-Golden, "The Quick Atmospheric Correction (QUAC) code: algorithm description and recent upgrades," *Opt. Eng*. 51(11), 111719 (2012).

[13] L.S. Bernstein, S.M. Adler-Golden, R.L. Sundberg, and A.J. Ratkowski, "In-scene-based atmospheric correction of uncalibrated VISible-SWIR (VIS-SWIR) hyper- and multispectral imagery," *Proc. SPIE Int. Soc. Opt. Eng*., 7107 (2008).

[14] T. Perkins, S. Adler-Golden, M. Matthew, A. Berk, G. Anderson, J. Gardner, G. Felde, "Retrieval of atmospheric properties from hyper and multispectral imagery with the FLAASH atmospheric correction algorithm," *Proc. SPIE 5979, Remote Sensing of Clouds and the Atmosphere X*, 59790E (31 October 2005); https://doi.org/10.1117/12.626526

[15] Baldridge, A. M., Hook, S. J., Grove, C. I. and Rivera, G.: TheASTER Spectral Library Version 2.0, *Remote Sens. Environ*.,113, 711–715, 2009.

[16] J.H. Gruninger, and R.L. Sundberg, "Determination of Spectral Components of Multispectral Images," in *Optical Remote Sensing of the Atmosphere*, Vol. 2, 1995, OSA Technical Digest Series (Optical Society of America, Washington DC, 1995), pp. 79-81.

[17] J.H. Gruninger, and R.L. Sundberg, "Bounds on Component Spectra of Multispectral Images" *Proceedings: Algorithms for Multispectral and Hyperspectral Imagery III*, V 3071 pp. 36-46 (1997).

[18] Moran, P. A. P. 1950. "Notes on Continuous Stochastic Phenomena." *Biometrika* 37 (1/2): 17–23. https://doi.org/10.2307/2332142.

[19] Dillon, W.R. and M. Godstein, *Multivariate analysis*, John Wiley & Sons, 1984.

[20] Thompson DR, Boardman JW, Eastwood ML, Green RO. A large airborne survey of Earth's visible-infrared spectral dimensionality. *Opt Express*. 2017 Apr 17;25(8):9186-9195. doi: 10.1364/OE.25.009186. PMID: 28437992.

[21] Shimansky, Y.P., "Continuous measure of significant linear dimensionality of a waveform set," *Computational statistics & data analysis*, **35**, 1-10, 2000.

[22] Kaiser, H.F., "The application of electronic computers to factor analysis," *Educational and Psychological Measurement*, XX, **1**, 141-151, 1960.

[23] Jolliffe, I.T., *Principal Component Analysis*, Springer-Verlag, 1986.

[24] S.S. Kraut, L.L. Scharf, and R.W. Butler, "The Adaptive Coherence Estimator: A uniformly most-powerful invariant adaptive detection statistic," *IEEE Trans. Signal Processing*, Vol. 53, No. 2 (2005).